




Freezing phase transition in hard-core lattice gases on the triangular lattice with exclusion up to seventh next-nearest neighbor

Asweel Ahmed A. Jaleel ^{1,2,3,*}, Dipanjan Mandal ^{4,†}, Jetin E. Thomas ^{1,2,‡} and R. Rajesh^{1,2,§}

¹*The Institute of Mathematical Sciences, CIT Campus, Taramani, Chennai 600113, India*

²*Homi Bhabha National Institute, Training School Complex, Anushakti Nagar, Mumbai 400094, India*

³*Department of Physics, Sadakathullah Appa College, Tirunelveli, Tamil Nadu 627011, India*

⁴*Department of Physics, University of Warwick, Coventry CV4 7AL, United Kingdom*



(Received 10 June 2022; accepted 5 August 2022; published 26 October 2022)

Hard-core lattice-gas models are minimal models to study entropy-driven phase transitions. In the k -nearest-neighbor lattice gas, a particle excludes all sites up to the k th next-nearest neighbors from being occupied by another particle. As k increases from one, it extrapolates from nearest-neighbor exclusion to the hard-sphere gas. In this paper we study the model on the triangular lattice for $k \leq 7$ using a flat histogram algorithm that includes cluster moves. Earlier studies focused on $k \leq 3$. We show that for $4 \leq k \leq 7$, the system undergoes a single phase transition from a low-density fluid phase to a high-density sublattice-ordered phase. Using partition function zeros and nonconvexity properties of the entropy, we show that the transitions are discontinuous. The critical chemical potential, coexistence densities, and critical pressure are determined accurately.

DOI: [10.1103/PhysRevE.106.044136](https://doi.org/10.1103/PhysRevE.106.044136)

I. INTRODUCTION

Hard-core lattice gases (HCLGs), a collection of particles on lattices that interact only through excluded volume interactions, are the simplest models to show phase transitions. In particular, they are minimal models to study fluid to solid freezing transitions induced by increasing density [1,2]. Since the interaction energies are either zero or infinity, temperature plays no role in such phase transitions. The phases and the nature of the transitions depend only on the shape of the excluded volume. To understand this dependence as well as the order in which the phases occur with increasing density, phase diagrams of many different shapes have been studied in detail in the literature. Examples include hard hexagons [3,4], triangles [5], squares [6–8], rectangles [9,10], tetraminos [11], rods [12–14], and plates [15,16].

Among the different shapes, a subclass of shapes of particular interest is the k -nearest-neighbor (NN) HCLG model in which the first k next-nearest neighbors of a particle are excluded from being occupied by another particle. The case $k = 1$ corresponds to nearest-neighbor exclusion, while the limit $k \rightarrow \infty$ corresponds to the well-studied hard-sphere problem in the continuum. Also, the model can be thought of as limiting cases of spin models with long-range interaction [17–20]. Introduced in the 1950s [6,21–26], the k -NN model, in addition to its relevance to critical phenomena and the hard-sphere gas, has found applications in diverse areas of research as well as direct experimental re-

alizations. Examples of applications include adsorption on surfaces [27–33], glass transitions [34–36], phase transitions in closely related HCLG models in which particles can have at most n nearest neighbors (also known as the Biroli-Mézard model [37]), attractive gases [38,39], and in combinatorial problems [40]. Some direct experimental realizations include porphyrins adsorbed on the Au(111) surface [41–43], adsorption of chlorine on a silver (100) surface [27], and adsorption of selenium on a nickel (100) surface [44].

In two dimensions, the phase diagram for the k -NN model for different k has been studied on the square, honeycomb, and triangular lattices using different techniques such as transfer-matrix calculations, high- and low-density expansions, and Monte Carlo simulations. We summarize the known results below.

On the square lattice, the model has been studied for $k \leq 11$, and a summary of known results may be found in Refs. [45–47]. For $k = 1, 3, 6, 7, 8, 9$, the model undergoes a single phase transition from a low-density fluid phase to a high-density sublattice-ordered phase. The transition is continuous for the 1-NN model and first order otherwise. The 2-NN and 5-NN models reduce to 2×2 and 3×3 hard-square problems, respectively, and the high-density phase has columnar order. The transition belongs to the Ashkin-Teller universality class for the 2-NN model and is discontinuous for the 5-NN model. The 4-NN, 10-NN, and 11-NN models show multiple phase transitions. The presence of multiple transitions are due to a sliding instability present in the high-density phase and also appear for $k > 11$ [46,48].

On the honeycomb lattice, the model has been studied for $k \leq 5$ [49–51]. The 1-NN model shows a single continuous transition, belonging to the Ising universality class, from a fluid to a sublattice-ordered phase. The 2-NN model shows a first-order transition, while the 3-NN model, surprisingly,

*asweel@sadakath.ac.in

†dipanjan.mandal@warwick.ac.uk

‡jetinthomas@imsc.res.in

§rjajesh@imsc.res.in

does not undergo any transition [49,50]. The 4-NN model shows a single continuous phase transition that belongs to the three-state Potts model. The 5-NN model has been shown to undergo two discontinuous transitions. However, these transitions show nonstandard scaling with system size [49].

The k -NN model on the triangular lattice, the main focus in this paper, has been studied for $k \leq 5$. The triangular lattice is of particular interest as it is a better approximation to the continuum than the square and honeycomb lattices. Thus, one would expect that phases seen in the continuum, like the hexatic phase, would be most easily seen on the triangular lattice. The 1-NN model on the triangular lattice is the hard-hexagon model. It is the only exactly solvable HCLG model and undergoes a transition from a disordered phase to a sublattice-ordered phase which belongs to the three-state Potts model [3,4,52]. The 2-NN model on a triangular lattice is known to show a single second-order transition which belongs to the four-state Potts model universality class [53–55]. The 3-NN model has been studied in detail recently and it undergoes a single discontinuous transition to a sublattice-ordered phase [55–57]. Using tensor renormalization group (TRG) methods, the 4-NN and 5-NN models were also studied. However, the phenomenology for the 4-NN and 5-NN models is not well established. The TRG results give a wide range of values for the critical chemical potential, and the nature of the transitions are also not clear [55]. Thus, compared to the square and honeycomb lattices, the k -NN model on the triangular lattice is less studied and it would be of interest to determine the phase diagram for the model for $k \geq 4$.

An additional motivation for studying the k -NN model on the triangular lattice comes from the algorithmic point of view. In general, Monte Carlo studies of HCLG models of particles with large excluded volume suffer from equilibration issues, especially at densities close to full packing. When only local moves are allowed, the system gets stuck in long-lived metastable states. Algorithms that include cluster moves can overcome these issues partially. One such algorithm is the grand canonical transfer-matrix-based strip cluster update algorithm (SCUA) that updates the configurations on strips that span the lattice in one attempt [13,58]. This algorithm has been very useful in obtaining the phase diagram of the k -NN model on square [46] and honeycomb [49] lattices as well as that of many other differently shaped particles [13,14,59–61]. However, the SCUA has difficulty in equilibrating systems which undergo a strong first-order transition close to full packing [56]. More recently, there have been two other algorithms that have proved useful. One is the TRG method, which was used to obtain the phase diagram for the k -NN model on the triangular lattice for $k \leq 5$ [55] and interacting hard equilateral triangles [50]. The other is the strip cluster Wang-Landau (SCWL) algorithm that combines the SCUA with flat histogram methods and thus determines the density of states for all densities [56,62]. A comparison of the efficacies of the TRG method and SCWL algorithm would be useful.

In this paper we study the k -NN model on the triangular lattice using flat histogram Monte Carlo simulations (SCWL algorithm) for $1 \leq k \leq 7$. We benchmark our simulations against the known exact solution of the 1-NN model. For the 2-NN model, we obtain improved estimates for the critical

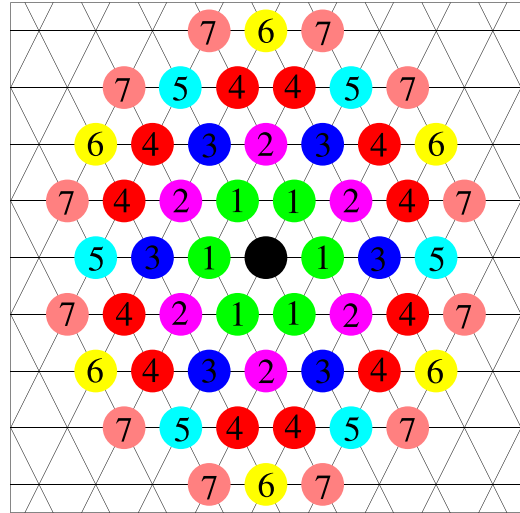


FIG. 1. The neighbors of the central site (black circle) are labeled according to the distance from it. The number in the circles denotes the range of exclusion k . In the k -NN exclusion model, a particle excludes all the sites with label less than or equal to k from being occupied by another particle.

density. For the 4-NN to 7-NN models, we show, using partition function zeros, that the system undergoes a single phase transition from a low-density fluid phase to a high-density sublattice-ordered phase. Based on the nonconvexity of the numerically obtained entropy, we show that the transitions are discontinuous. The estimates for the critical parameters are summarized in Table III. In addition, we show that, compared to the TRG method, the SCWL algorithm is able to obtain more accurate results for larger k .

The remainder of the paper is organized as follows. In Sec. II we define the k -NN model and outline the SCWL algorithm adapted to the k -NN model on the triangular lattice. In Sec. III we first benchmark the simulations with known results from the 1-NN and 2-NN models. We also describe the results for the 2-NN model as well for 4-NN to 7-NN models. Section IV contains a summary and discussion of the results.

II. MODEL AND MONTE CARLO ALGORITHM

A. The k -NN hard-core lattice gas

Consider an $L \times L$ triangular lattice with periodic boundary conditions. A lattice site can be occupied by at most one particle. In the k -NN exclusion model, a particle excludes all the sites up to the k -th nearest neighbors from being occupied by another particle. Figure 1 shows the excluded neighbors of a particle for $k = 1, 2, \dots, 7$. The number of excluded sites N_{excl} and the maximum number density n_{max} for a given k are given in Table I.

B. Monte Carlo algorithm

We study the k -NN model using the strip cluster Wang-Landau algorithm introduced recently [56,62]. For the sake of completeness, as well as to explain the generalization of the algorithm to general k , we briefly describe the algorithm below.

TABLE I. For each k , the number of neighbors that are excluded from being occupied by a particle N_{excl} , the maximum number density n_{max} , the orientation of the rows, and the range of exclusion δ , as defined for the evaporation and deposition algorithm (see the text in Sec. II B), are tabulated.

k	N_{excl}	n_{max}	Orientation of rows	δ
1	6	1/3	$0, \pi/3, 2\pi/3$	1
2	12	1/4	$0, \pi/3, 2\pi/3$	1
3	18	1/7	$0, \pi/3, 2\pi/3$	2
4	30	1/9	$0, \pi/3, 2\pi/3$	2
5	36	1/12	$0, \pi/3, 2\pi/3$	3
6	42	1/13	$\pi/6, \pi/2, 5\pi/6$	2
7	54	1/16	$0, \pi/3, 2\pi/3$	3

In the SCWL algorithm, rejection-free cluster moves are combined with the Wang-Landau flat histogram algorithm [63,64] for estimating the density of states $g(N, L)$, where N is the number of particles. We first outline the Wang-Landau protocol.

The weight of a configuration with N particles is taken to be inversely proportional to $g(N, L)$. A histogram $H(N)$ records the number of times configurations with N particles are visited during the simulations. Initially, $H(N) = 0$ and $S(N) = 0$, where $S(N)$ is the entropy

$$S(N) = \ln g(N, L). \quad (1)$$

The system evolves via an evaporation-deposition algorithm (described below). After every microstep, if there are N particles, then $H(N) = H(N) + 1$ and $S(N) = S(N) + f$, where f is a modification factor. The system is evolved until the histogram becomes reasonably flat, i.e., $H_{\text{min}}(N) > c \times H_{\text{max}}(N)$, where H_{min} and H_{max} are the minimum and maximum values of the histogram, respectively, and c is a constant. In our simulations, we choose $c = 0.80$. This is one iteration of the Wang-Landau algorithm. The modification factor f is halved for the next iteration and the histogram $H(N)$ is reset to zero. Initially, f is chosen to be equal to 1. The iterations are continued until f is less than a predefined limit f_{min} . In our simulations $f_{\text{min}} = 2^{-22}$.

We now outline the cluster move for evaporating and depositing particles [56,62]. A row is selected at random. The orientations of the rows depend on k and are as tabulated in Table I. Some of the lattice sites in the row are excluded from occupation due to particles in nearby rows. These excluded sites break up the row into open segments. We note that the orientations of the rows, as given in Table I, are chosen such that the filling of these segments is independent.

Choose a segment at random. Let this segment have ℓ sites. Remove all the particles in the segment and let there be N_0 particles remaining in the system. Along this row, there has to be a minimum of δ empty sites between two particles. The values of δ for different k are given in Table I. It is possible to occupy $0, 1, \dots, n^*$ particles, where $n^* = (\ell + \delta)/(\delta + 1)$. The refilling is done in two steps: First we determine the number of particles n that should be deposited and second we choose a random configuration from all possible ways of placing n particles in ℓ sites.

The probability of choosing n particles to deposit is

$$\text{Prob}_o(\ell, n) = \frac{C_o(\ell, n)/g(N_0 + n, L)}{\sum_{i=0}^{n^*} C_o(\ell, i)/g(N_0 + i, L)}, \quad (2)$$

where $C_o(\ell, n)$ is the number of ways of placing n particles on a segment of length ℓ sites with open boundary conditions. If there are no sites excluded in an entire row, then we have to use periodic boundary condition for deposition. Then the probability $\text{Prob}_p(\ell, n)$ of choosing n particles to deposit is

$$\text{Prob}_p(\ell, n) = \frac{C_p(\ell, n)/g(N_0 + n, L)}{\sum_{i=0}^{n^*} C_p(\ell, i)/g(N_0 + i, L)}, \quad (3)$$

where $C_p(\ell, n)$ is the number of ways of placing n particles on a ring of ℓ sites and $n^* = \ell/(\delta + 1)$.

Determining $C_o(\ell, n)$ and $C_p(\ell, n)$ is a straightforward enumeration problem and is given by

$$C_o(\ell, n) = \frac{(\ell + \delta - n\delta)!}{(\ell + \delta - n\delta)!n!}, \quad n = 0, 1, \dots, \left\lfloor \frac{\ell + \delta}{\delta + 1} \right\rfloor, \quad (4)$$

$$C_p(\ell, n) = \frac{\ell(\ell - n\delta - 1)!}{(\ell - n\delta - n)!n!}, \quad n = 0, 1, \dots, \left\lfloor \frac{\ell}{\delta + 1} \right\rfloor. \quad (5)$$

After determining n , we fill the segment iteratively from one end to the other. For open segments, the probability $P_o(\ell, n)$ that the first site is empty is given by

$$P_o(\ell, n) = \frac{C_o(\ell - 1, n)}{C_o(\ell, n)} = \frac{\ell + \delta - n\delta - n}{\ell + k - n\delta}. \quad (6)$$

If the first site is empty, the ℓ is reduced by one, keeping n the same, and the step is repeated. If the first site is occupied, then $\ell \rightarrow \ell - \delta$, $n \rightarrow n - 1$, and the step is repeated. If the segment has periodic boundary conditions, the probability $P_p(\ell, n)$ that the first δ sites are empty is given by

$$P_p(\ell, n) = \frac{C_o(\ell - \delta, n)}{C_p(\ell, n)} = \frac{\ell - n\delta}{\ell}. \quad (7)$$

If the first δ sites are empty, then it reduces to an open segment of length $\ell - \delta$ with n particles. Otherwise, one of the first δ sites, chosen at random, is occupied and it reduces to an open segment of length $\ell - 2\delta - 1$ with $n - 1$ particles. The values of $C_o(\ell, n)$, $C_p(\ell, n)$, $P_o(\ell, n)$, and $P_p(\ell, n)$ do not change during the simulation and are therefore evaluated once in the beginning and stored as a lookup table. The values of entropy, order parameter, susceptibility, etc., reported in the paper are those calculated at the last Wang-Landau iteration.

III. RESULTS

We now describe the results from the flat histogram simulations. For $k = 1$, the hard-hexagon model, an exact solution is available and we benchmark our simulations against the known results. For $k = 2$, we compare our results with those from earlier simulations. For $k = 3$, our recent results can be found in Ref. [56]. For $k = 4, 5, 6, 7$, we present new results.

We start by defining different thermodynamic quantities. Knowing the density of states $g(N, L)$, the grand canonical

partition function $\mathcal{L}(\mu, L)$, the pressure P , and the average values of any observable \mathcal{O} are given by

$$\mathcal{L}(\mu, L) = \sum_{N=0}^{N_{\max}} g(N, L) e^{\mu N}, \quad (8)$$

$$P(\mu) = \frac{1}{L^2} \ln \mathcal{L}(\mu, L), \quad (9)$$

$$\langle \mathcal{O} \rangle = \frac{\sum_N \mathcal{O}(N) g(N, L) e^{\mu N}}{\mathcal{L}(\mu, L)}, \quad (10)$$

where μ is the reduced chemical potential. At a particular density $\rho = N/n_{\max}$, the pressure in the canonical ensemble, $\tilde{P}(\rho)$, is calculated as [65,66]

$$\tilde{P}(\rho) = \int_0^\rho [1 - \phi(\rho)] \frac{\partial}{\partial \rho} \left[\frac{\rho}{1 - \phi(\rho)} \right] d\rho, \quad (11)$$

where $\phi(\rho)$ is the mean fraction of sites where a new particle cannot be placed because of exclusion due to existing particles.

For all the models, we will show that the model undergoes a single transition from a disordered fluid phase to a high-density solid phase. In the solid phase, the particles occupy one of N_{sub} sublattices. It is clear that $N_{\text{sub}} = 1/n_{\max}$, where the maximum number density n_{\max} for each k is as tabulated in Table I. We define the sublattice order parameter for a given k to be

$$q_k = \left[\sum_{j=1}^{N_{\text{sub}}} \rho_j \exp \left[\frac{2\pi i(j-1)}{N_{\text{sub}}} \right] \right], \quad (12)$$

where ρ_j is the density of particles in sublattice j . Compressibility κ_k and susceptibility χ_k are

$$\kappa_k = L^2 [\langle \rho_k^2 \rangle - \langle \rho_k \rangle^2], \quad (13)$$

$$\chi_k = L^2 [\langle q_k^2 \rangle - \langle q_k \rangle^2]. \quad (14)$$

For the numerical analysis, it is useful to define an associated quantity t_k as

$$t_k = \frac{\partial \ln \langle q_k \rangle}{\partial \mu}. \quad (15)$$

From finite-size scaling [67–69], the above thermodynamic quantities at the transition point scale with L as

$$\begin{aligned} \kappa_k(\mu_c) &\sim L^{\alpha/\nu}, & \langle q_k(\mu_c) \rangle &\sim L^{-\beta/\nu}, \\ \chi_k(\mu_c) &\sim L^{\gamma/\nu}, & t_k &\sim L^{1/\nu}, \end{aligned} \quad (16)$$

where α , β , γ , and ν are critical exponents. For a first-order transition in two dimensions, $\nu = 1/2$ and $\alpha/\nu = \beta/\nu = \gamma/\nu = 2$.

Let μ_c , ρ_c , and P_c denote the critical chemical potential, critical density, and critical pressure in the thermodynamic limit. For a finite-size system, the deviation of these quantities from the thermodynamic limit varies as

$$x_c(L) - x_c \sim L^{-1/\nu}, \quad x = \mu, \rho, P. \quad (17)$$

For the first-order transitions, we use the following analysis. We use the loci of the zeros of the partition function to determine the number of phase transitions. The nature of the

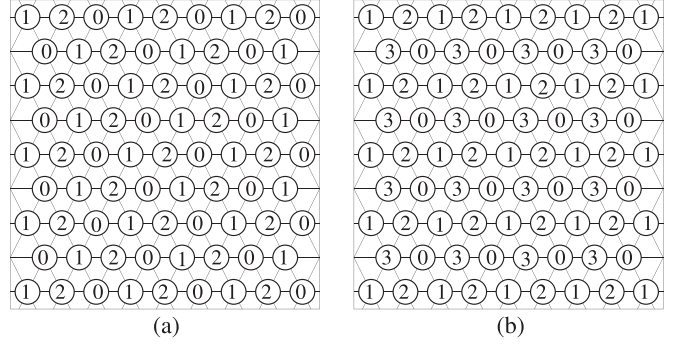


FIG. 2. Division of lattice sites into sublattices for the (a) 1-NN model (three sublattices) and (b) 2-NN model (four sublattices).

transition is established from the angle at which the zeros approach the real axis, as well as the nonconvexity properties of the entropy. Here $\mu_c(L)$ is obtained from the partition function zeros, analysis of the nonconvex (NC) behavior of the entropy (see Sec. III D and Refs. [56,62] for details), and the value of μ at which susceptibility is maximum. The coexistence densities $\rho_f(L)$ and $\rho_s(L)$ of the first-order transition are also estimated from NC analysis.

To estimate the critical behavior accurately, the relevant thermodynamic quantities are calculated with a step size of $\Delta\mu = 10^{-5}$. Errors in each data point are standard errors obtained from 16 independent simulations using different sequences of random numbers. Errors in the final estimate of critical parameters are fitting errors.

A. The 1-NN model

The 1-NN model, or the hard-hexagon model, is exactly solvable [3,4]. There is a single continuous phase transition from a disordered phase to the sublattice phase with increasing particle density. In the ordered phase, particles preferentially occupy one of the three sublattices shown in Fig. 2(a). The critical parameters are $\mu_c = \ln \left[\frac{1}{2}(11 + 5\sqrt{5}) \right] = 2.4060 \dots$, $\rho_c = \frac{3}{10}(5 - \sqrt{5}) = 0.82917 \dots$, $\alpha = 1/3$, $\beta = 1/9$, $\gamma = 13/9$, and $\nu = 5/6$ [3]. The phase transition belongs to the three-state Potts model universality class. In addition, the density and compressibility, for $\rho > \rho_c$, vary with μ as [52]

$$\begin{aligned} \mu(\rho) &= \ln[2(\rho - 2)(3 - \rho)^3] \\ &\quad - \ln[(27 - 108\rho + 135\rho^2 - 66\rho^3 + 11\rho^4) \\ &\quad + (-9 + 15\rho - 5\rho^2)^{3/2}(-1 + 3\rho - \rho^2)^{1/2}], \end{aligned} \quad (18)$$

$$\begin{aligned} \kappa(\rho) &= \frac{1}{15}[(3 - 2\rho)(-1 + 3\rho - \rho^2)^{1/2} \\ &\quad \times (-9 + 15\rho - 5\rho^2)^{-1/2} - (-1 + 3\rho - \rho^2)]. \end{aligned} \quad (19)$$

To benchmark our flat histogram simulations, we compare the numerically obtained density and compressibility for $\rho > \rho_c$ with the exact results in Eqs. (18) and (19), as shown in Figs. 3(a) and 3(b), respectively. The numerical results are in excellent agreement with the exact results except near the critical point, where the numerical results deviate from the exact result for the infinite system due to finite-size effects.

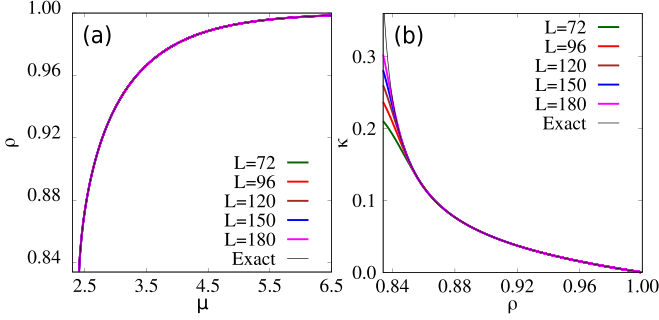


FIG. 3. Comparison of the numerically obtained (a) density ρ and (b) compressibility κ for the 1-NN model with the exact results as given in Eqs. (18) and (19) for $\rho > \rho_c$. Data for different system sizes are shown.

We estimate the exponents using the scaling laws in Eq. (16), as shown in Fig. 4. We obtain $1/\nu \approx 1.21(1)$, $\beta/\nu \approx 0.134(2)$, and $\gamma/\nu \approx 1.737(6)$. These estimates are in good agreement with the exact value of the exponents $1/\nu = 1.2$, $\beta/\nu = 0.133\dots$, and $\gamma/\nu = 1.733\dots$. We determine the critical chemical potential μ_c and critical density ρ_c by extrapolating the $\mu_c(L)$ and $\rho_c(L)$ to infinite systems size using Eq. (17). Here $\mu_c(L)$ is identified as the μ at which χ is maximum and $\rho_c(L)$ is the corresponding density. The extrapolation is shown in Fig. 5. We obtain $\mu_c \approx 2.4064(6)$

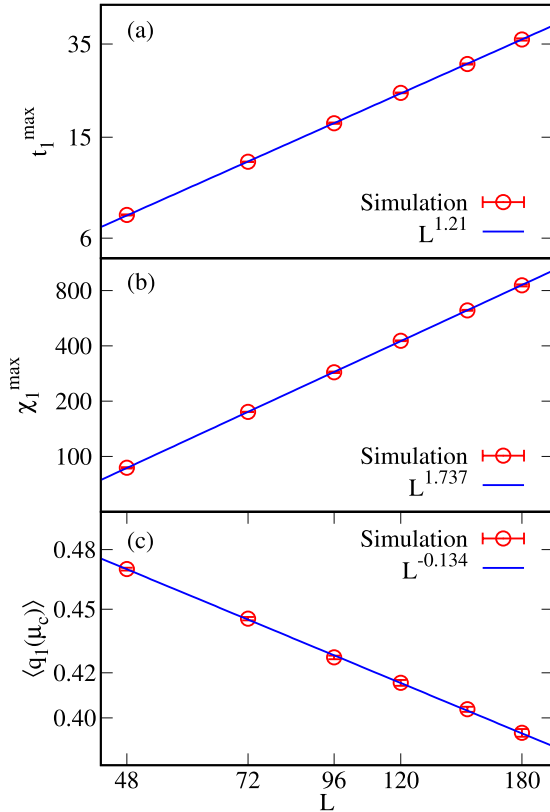


FIG. 4. Power-law scaling of (a) t_1^{\max} , (b) χ_1^{\max} , and (c) $\langle q_1(\mu_c) \rangle$ with system size L for the 1-NN model. The solid straight lines are best fits to the data.

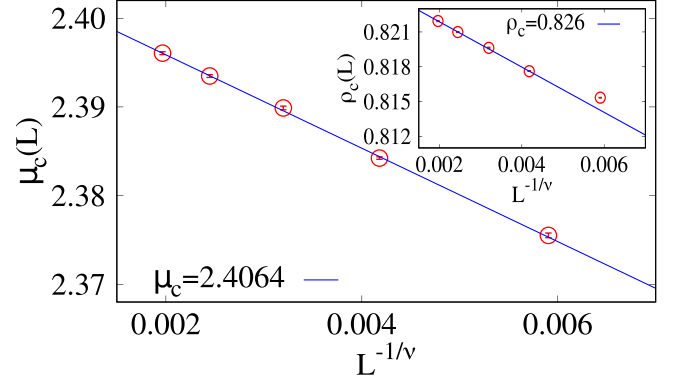


FIG. 5. Extrapolation of $\mu_c(L)$ and $\rho_c(L)$ (inset) to infinite system size using the scaling in Eq. (17). The data are for the 1-NN model and we have chosen $\nu = 5/6$. In the extrapolation of $\rho_c(L)$ we have used the data for only $L \geq 96$.

and $\rho_c \approx 0.826(4)$, which are in good agreement with the exact results $2.4060\dots$ and $0.82917\dots$.

In addition to these checks, we also confirm that the entropies of the fully packed state and the state with one vacancy are reproduced correctly in the simulations. Based on the above results, we conclude that the SCWL algorithm can accurately obtain the entropy for all densities.

B. The 2-NN model

The 2-NN model is known to exhibit a single continuous phase transition from a disordered phase to a sublattice-ordered phase. In the ordered phase, the particles preferentially occupy one of the four sublattices shown in Fig. 2(b). Due to the breaking of the fourfold symmetry, the phase transition is expected to belong to the universality class of the four-state Potts model. The exact values of critical exponents for the four-state Potts model are $\alpha = 2/3$, $\beta = 1/12$, $\gamma = 7/6$, and $\nu = 2/3$ [70].

The 2-NN model has been studied earlier using different numerical methods. The known estimates for μ_c are approximately equal to 1.75989 from transfer-matrix scaling [53], 1.75682(2) using Monte Carlo simulations [54], 1.75587 using transfer-matrix methods [55], and 1.75398 using tensor renormalization group method [55]. The corresponding values for ρ_c are 0.74856 [53] and 0.72(2) [54]. The numerical estimation of the critical exponents has convergence issues due to logarithm corrections, both additive and multiplicative, that are present for the four-state Potts model [71]. The earlier estimates for the critical exponents of the 2-NN model were $\nu = 0.72$ and $\beta/\nu = 1.115$ from transfer-matrix scaling [53] and $1/\nu = 1.51(1)$ and $\beta/\nu = 0.1257(7)$ from Monte Carlo simulations [54].

We estimate the critical exponents for the 2-NN model using the scaling laws in Eq. (16), as shown in Fig. 6. We obtain $1/\nu = 1.48(2)$, $\beta/\nu \approx 0.124(3)$, and $\gamma/\nu \approx 1.812(8)$. The known exact value of the exponents are $1/\nu = 1.5$, $\beta/\nu = 0.125$, and $\gamma/\nu = 1.75$. The value of γ/ν is overestimated, possibly because of ignoring logarithmic corrections.

We determine the critical chemical potential μ_c and critical density ρ_c by extrapolating $\mu_c(L)$ and $\rho_c(L)$ to infinite

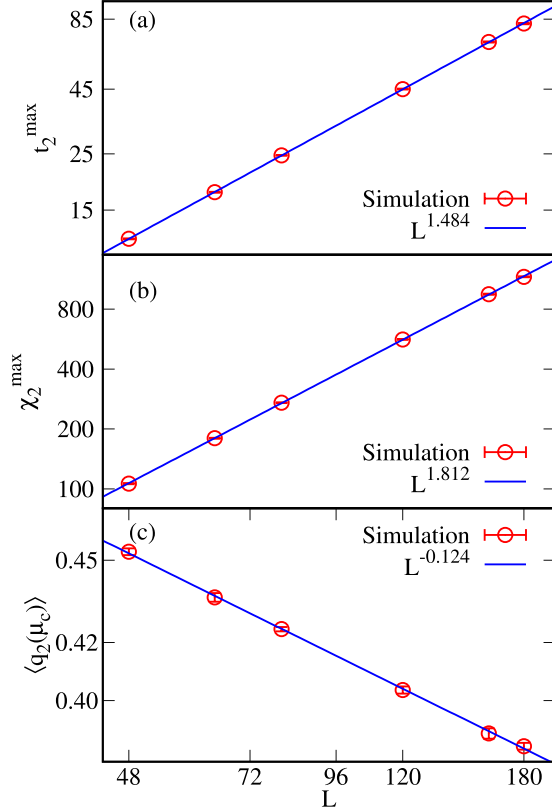


FIG. 6. Power-law scaling of (a) t_2^{\max} , (b) χ_2^{\max} , and (c) $\langle q_2(\mu_c) \rangle$ with system size L for the 2-NN model. The solid straight lines are best fits to the data.

systems size using Eq. (17). The extrapolation is shown in Fig. 7. We obtain $\mu_c = 1.7568(4)$ and $\rho_c = 0.7419(5)$. Our estimate for μ_c is consistent with earlier estimates (see above). For ρ_c , the estimate is closer to the transfer-matrix estimate of 0.74856 [53] rather than the more recent Monte Carlo estimate of 0.72(2) [54]. From the inset of Fig. 7, it can be seen that even for the smallest system size $\rho_c(L) > 0.725$.

C. The 3-NN model

The 3-NN model has been studied using matrix methods and series expansion [26], tensor renormalization group

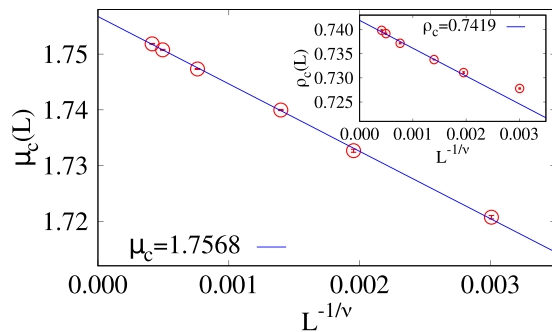


FIG. 7. Extrapolation of $\mu_c(L)$ and $\rho_c(L)$ (inset) to infinite system size using the scaling in Eq. (17). The data are for the 2-NN model and we have chosen $\nu = 2/3$.

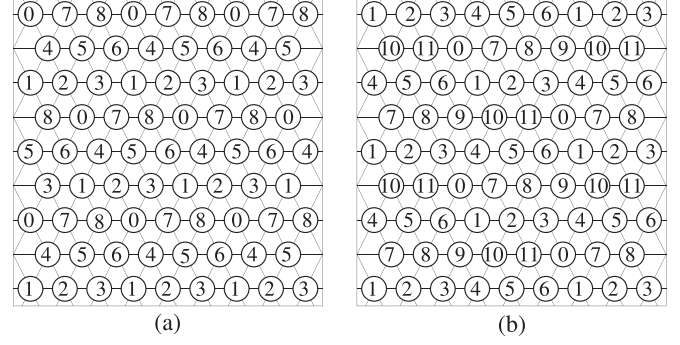


FIG. 8. Division of lattice sites into sublattices for the (a) 4-NN model (9 sublattices) and (b) 5-NN model (12 sublattices).

method [55], evaporation-deposition algorithms [57], and the SCWL algorithm [56]. The model shows a single first-order transition from a disordered phase to a sublattice-ordered phase. Based on SCWL algorithm, we recently found that $\mu_c = 4.4641(3)$ and the critical pressure is $P_c = 0.6397(1)$. Both phases coexist between densities $\rho_f = 0.8482(1)$ and $\rho_s = 0.9839(2)$ [56]. A detailed discussion of the analysis as well as a summary of past work can be found in Ref. [56].

D. The 4-NN model

Compared to 1-NN, 2-NN, and 3-NN models, there is not much known for $k \geq 4$. The 4-NN model has been studied earlier using the tensor renormalization group method [55]. It was concluded that the 4-NN model shows a continuous phase transition with μ_c between 2.65 and 2.7.

We now present our results for the 4-NN model in detail. We will follow a similar analysis for larger k .

At full packing, the particles occupy one of the $N_{\text{sub}} = 9$ sublattices shown in Fig. 8(a). We first show that there is only one phase transition from a disordered fluid phase to the high-density sublattice-ordered phase.

To do so, we examine the loci of zeros of the partition function in the complex z plane. Figure 9 shows the zeros for $L = 216$. The partition function zeros (PFZs) pinch the real axis at only one point, showing the presence of only a single phase transition. The locus forms a circle; hence the angle it makes with the real axis is $\pi/2$, suggesting that the transition is discontinuous [72,73].

The first-order nature of the transition can be further established by showing that the entropy is nonconvex in certain regions [56,62]. Figure 10 shows the nonconvex part of the entropy for $L = 36$ and the corresponding convex envelope, shown by the solid line. Analysis of the nonconvexity gives a precise estimate of critical parameters of the first-order transition [56,62]. Let N_f and N_s denote the number of particles at the end points of the convex envelope on the fluid side and sublattice side, respectively (see Fig. 10). Then $\rho_f(L) = N_f/L^2 \times N_{\text{sub}}$ and $\rho_s(L) = N_s/L^2 \times N_{\text{sub}}$ are the densities at the boundaries of the coexistence regime. The critical chemical potential

$$\mu_c(L) = -\frac{S(N_s) - S(N_f)}{N_s - N_f} \quad (20)$$

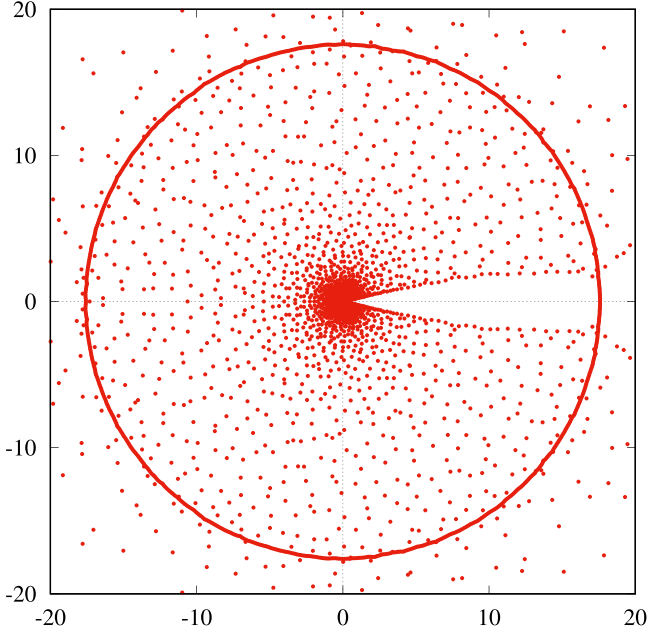


FIG. 9. Zeros of the grand canonical partition function in the complex z plane ($z = e^\mu$) for the 4-NN model. The locus of the zeros forms a circle and pinches the positive real axis only at one point. The data are for $L = 216$.

is the slope of the convex envelope. The system-size-dependent critical parameters $\rho_f(L)$, $\rho_s(L)$, and $\mu_c(L)$ thus obtained are tabulated in Table II for different system sizes. The convergence to the infinite system size is rapid.

Figure 11 shows the extrapolation of $\mu_c(L)$ to infinite system size using Eq. (17) with $\nu = 2$. We determine $\mu_c(L)$ from the maximum of χ , NC analysis, and the position of the PFZs closest to the origin. We obtain $\mu_{c,4} = 2.8696(2)$ from NC analysis and $\mu_{c,4} = 2.8697(2)$ from susceptibility and PFZs. The coexistence densities are found to $\rho_{f,4} = 0.7404(2)$ and $\rho_{s,4} = 0.9067(2)$ from NC analysis (extrapolation not shown). The critical pressure is estimated to be $P_{c,4} = 0.3262(2)$. Further results for the dependence of density, order parameter,

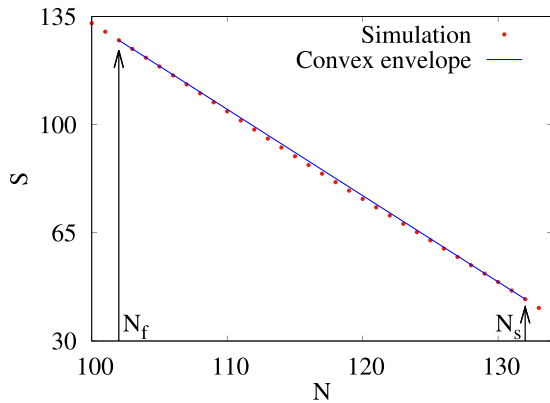


FIG. 10. Nonconvex part of the entropy and the corresponding convex envelope construction for the 4-NN model. The black solid arrows show the locations of N_f and N_s . The significance of N_f and N_s is explained in the text.

TABLE II. Critical parameters from nonconvexity in entropy of the 4-NN model. The last row shows the results of extrapolation performed against $1/L^2$ using linear regression (see Fig. 11).

L	ρ_f	ρ_s	μ_c
108	0.7319(1)	0.9094(1)	2.8593(1)
117	0.7331(1)	0.9090(1)	2.8606(1)
126	0.7340(1)	0.9089(1)	2.8632(1)
135	0.7347(1)	0.9085(1)	2.8632(1)
144	0.7356(1)	0.9086(1)	2.8643(1)
153	0.7358(1)	0.9081(1)	2.8644(1)
162	0.7364(1)	0.9080(1)	2.8651(1)
171	0.7366(1)	0.9077(1)	2.8655(1)
180	0.7374(1)	0.9077(1)	2.8661(1)
189	0.7376(1)	0.9076(1)	2.8663(1)
198	0.7379(1)	0.9076(1)	2.8666(1)
207	0.7382(1)	0.9075(1)	2.8669(1)
216	0.7384(1)	0.9072(1)	2.8671(1)
225	0.7386(1)	0.9073(1)	2.8675(1)
∞	0.7404(1)	0.9067(1)	2.8696(1)

Binder cumulant, and pressure with chemical potential μ can be found in the Supplemental Material [74] under Sec. 4-NN.

Note that our analysis shows that the transition is first order. This is in contradiction to that obtained from the TRG method, where it was concluded that the transition is continuous. Also, our estimate of $\mu_c = 2.8696(2)$ is outside the range of 2.65 and 2.7 estimated using the TRG method in Ref. [55]. The better accuracy is presumably due to the SCWL algorithm accessing the high-density states in an efficient manner.

E. The 5-NN model

In the 5-NN model, at full packing, the particles occupy one of the $N_{\text{sub}} = 12$ sublattices shown in Fig. 8(b). In earlier work it was argued, based on the tensor renormalization group, that the model exhibits a single first-order transition with μ_c roughly in the range $4.4 < \mu_c < 4.5$ [55].

The analysis we present for the 5-NN model (and higher k) is the same as that of the 4-NN model, so we only summarize

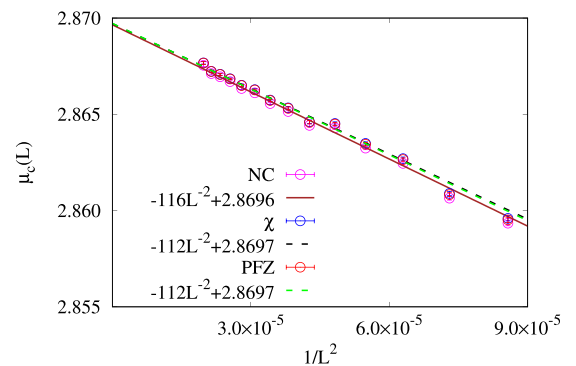


FIG. 11. Variation of the critical chemical potential $\mu_c(L)$ with system size L for the 4-NN model. The data were obtained from nonconvexity analysis, susceptibility χ , and partition function zeros. The error in each data point was obtained from 16 independent simulations. Solid and dashed lines are the best linear fits to the data.

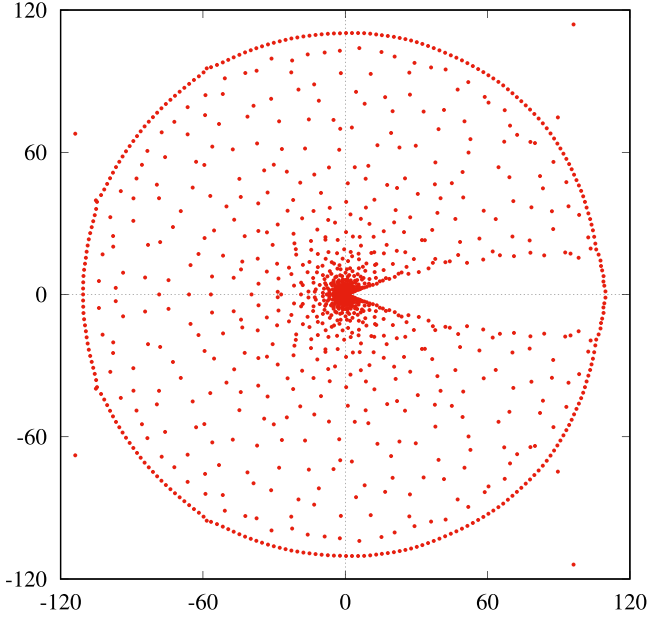


FIG. 12. Zeros of the grand canonical partition function in the complex z plane ($z = e^\mu$) for the 5-NN model. The locus of the zeros forms a circle and pinches the positive real axis only at one point.

the results. We simulate system sizes up to $L = 180$. We first show that there is only one phase transition from a disordered fluid phase to the high-density sublattice-ordered phase. Figure 12 shows the PFZs for $L = 180$. The locus of the zeros forms a circle and pinch the real axis at only one point. We conclude that there is only one phase transition in the system. Since the locus is a circle, the angle of approach of the leading zeros is $\pi/2$, suggesting that the transition is discontinuous. We note that for smaller L , the PFZs of the 5-NN model also form an inner circle. However, as L increases, these two circles merge and become indistinguishable.

We find that the entropy is nonconvex, giving direct proof of the first-order nature of the transition. From the NC analysis, we obtain $\rho_f(L)$, $\rho_s(L)$, and $\mu_c(L)$ for different system sizes. Figure 13 shows the extrapolation to the infinite system size of $\mu_c(L)$ obtained from nonconvexity analysis, PFZs, and

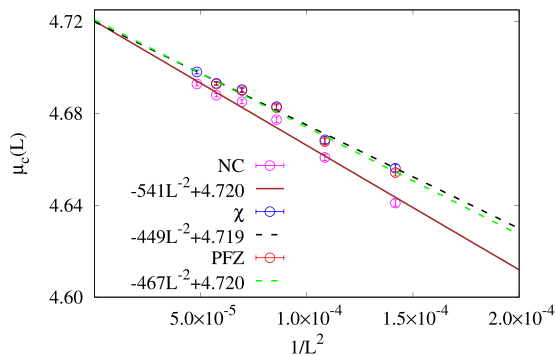


FIG. 13. Variation of the critical chemical potential $\mu_c(L)$ with system size L for the 5-NN model. The data were obtained from nonconvexity analysis, susceptibility χ , and partition function zeros. The error in each data point was obtained from 16 independent simulations. Solid and dashed lines are the best linear fits to the data.

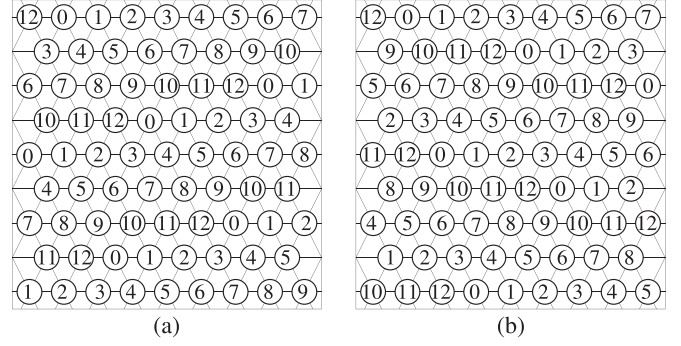


FIG. 14. Division of lattice sites into sublattices for the 6-NN model (13 sublattices). The division can be done in two equivalent ways as shown in (a) and (b).

the peak position of susceptibility. The critical chemical potential was estimated to be $\mu_{c,5} = 4.720(3)$ from NC analysis and PFZ data and $\mu_{c,5} = 4.720(1)$ from susceptibility. The end points of the coexistence regime were similarly found to be $\rho_{f,5} = 0.916(3)$ and $\rho_{s,5} = 0.988(3)$ from the NC analysis. We obtain the critical pressure to be $P_{c,5} = 0.3942(2)$. Further results for the dependence of density, order parameter, Binder cumulant, and pressure with chemical potential μ can be found in the Supplemental Material [74] under Sec. 5-NN.

Note that our analysis shows that the transition is first order, consistent with preliminary results obtained using the TRG method [55]. Also, our estimate of $\mu_c = 4.720(3)$ is outside the range of $4.4 < \mu_c < 4.5$ obtained in Ref. [55].

F. The 6-NN model

In the 6-NN model, at full packing, the particles occupy one of the $N_{\text{sub}} = 13$ sublattices shown in Fig. 14. The lattice can be divided into 13 sublattices in two different ways, which we call type-A and type-B, as shown in Fig. 14. The nature and location of the transition is not known for this model as it has not been studied earlier.

We simulate system sizes up to $L = 169$. We first show that there is only one phase transition from a disordered fluid phase to the high-density sublattice-ordered phase. In Fig. 15 we show the PFZs for $L = 169$. The locus of the zeros forms a circle and pinch the real axis at only one point. We conclude that there is only one phase transition in the system. Since the locus is a circle, the angle of approach of the leading zeros is $\pi/2$, suggesting that the transition is discontinuous.

We find that the entropy is nonconvex, giving direct proof of the first-order nature of the transition. From the NC analysis, we obtain $\rho_f(L)$, $\rho_s(L)$, and $\mu_c(L)$ for different system sizes. Figure 16 shows the extrapolation to the infinite system size of $\mu_c(L)$ obtained from nonconvexity analysis, PFZs, and the peak position of susceptibility. The critical chemical potential is estimated to be $\mu_{c,6} = 4.2574(4)$ from nonconvexity analysis and susceptibility and $\mu_{c,6} = 4.2575(4)$ from PFZ data. The end points of the coexistence regime were similarly found to be $\rho_{f,6} = 0.7898(1)$ and $\rho_{s,6} = 0.9818(2)$ from the NC analysis. We obtain the critical pressure to be $P_{c,6} = 0.3287(1)$. Further results for the dependence of density, order parameter, Binder cumulant, and pressure with chemical

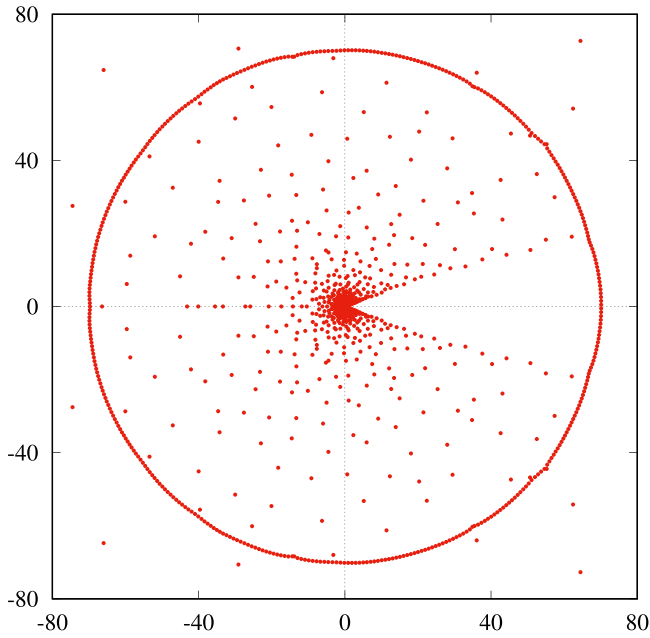


FIG. 15. Zeros of the grand canonical partition function in the complex z plane ($z = e^\mu$) for the 6-NN model. The locus of the zeros forms a circle and pinches the positive real axis only at one point.

potential μ can be found in the Supplemental Material [74] under Sec. 6-NN.

G. The 7-NN model

In the 7-NN model, at full packing, the particles occupy one of the $N_{\text{sub}} = 16$ sublattices shown in Fig. 17. The nature and location of transition are not known for this model as it has not been studied earlier.

We simulate system sizes up to $L = 192$. We first show that there is only one phase transition from a disordered fluid phase to the high-density sublattice-ordered phase. In Fig. 18 we show the PFZs for $L = 192$. The locus of the zeros forms a circle and pinch the real axis at only one point. We conclude that there is only one phase transition in the system. Since the

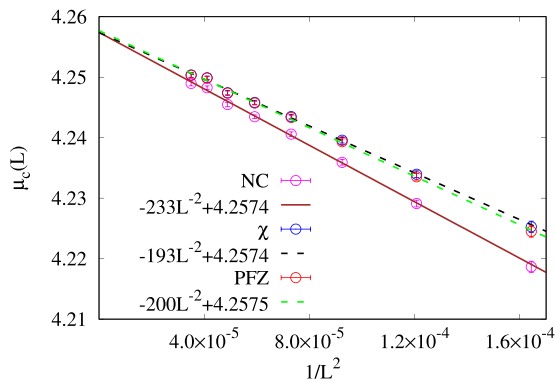


FIG. 16. Variation of the critical chemical potential $\mu_c(L)$ with system size L for the 6-NN model. The data were obtained from nonconvexity analysis, susceptibility χ , and partition function zeros. The error in each data point was obtained from 16 independent simulations. Solid and dashed lines are the best linear fits to the data.

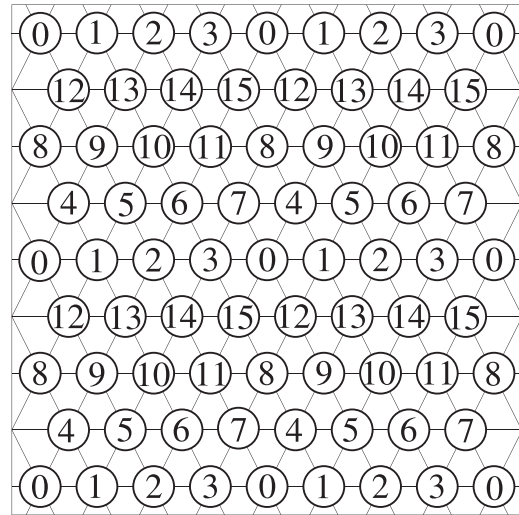


FIG. 17. Division of lattice sites into sublattices for the 7-NN model (16 sublattices).

locus is a circle, the angle of approach of the leading zeros is $\pi/2$, suggesting that the transition is discontinuous.

We find that the entropy is nonconvex, giving direct proof of the first-order nature of the transition. From the NC analysis, we obtain $\rho_f(L)$, $\rho_s(L)$, and $\mu_c(L)$ for different system sizes. Figure 19 shows the extrapolation to the infinite system size of $\mu_c(L)$ obtained from nonconvexity analysis, PFZs, and the peak position of susceptibility. The critical chemical potential was estimated to be $\mu_{c,7} = 3.9326(8)$ from nonconvexity analysis, $\mu_{c,7} = 3.9328(8)$ from susceptibility, and $\mu_{c,7} = 3.9329(7)$ from PFZ data. The end points of the coexistence regime were similarly found to be $\rho_{f,7} = 0.7469(4)$

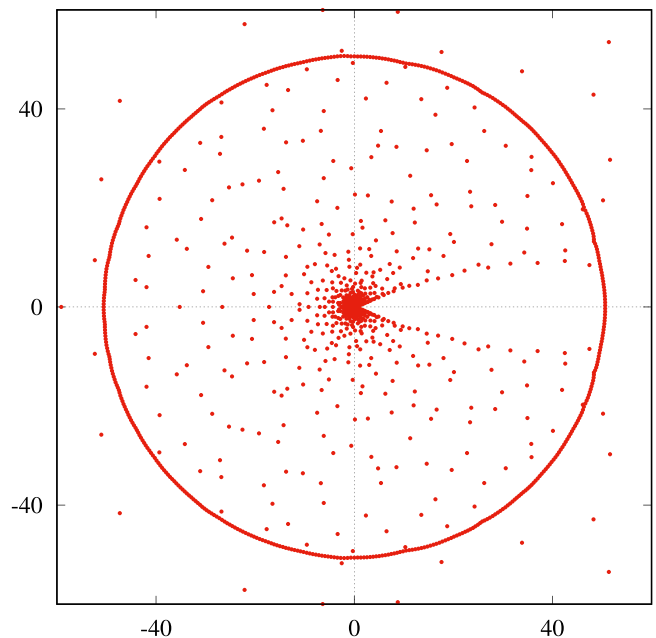


FIG. 18. Zeros of the grand canonical partition function in the complex z plane ($z = e^\mu$) for the 7-NN model. The locus of the zeros forms a circle and pinches the positive real axis only at one point.

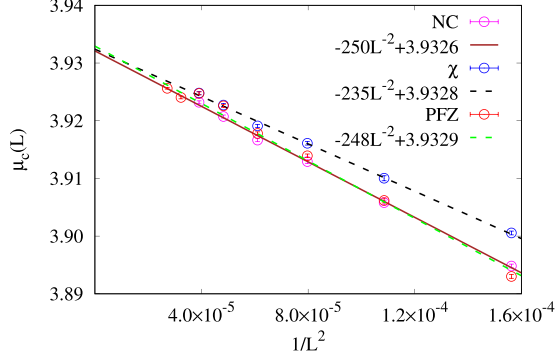


FIG. 19. Variation of the critical chemical potential $\mu_c(L)$ with system size L for the 7-NN model. The data were obtained from nonconvexity analysis, susceptibility χ , and partition function zeros. The error in each data point was obtained from 16 independent simulations. Solid and dashed lines are the best linear fits to the data.

and $\rho_{s,7} = 0.9709(3)$ from the NC analysis. We obtain the critical pressure to be $P_{c,7} = 0.2471(1)$. Further results for the dependence of density, order parameter, Binder cumulant, and pressure with chemical potential μ can be found in the Supplemental Material [74] under Sec. 7-NN.

IV. SUMMARY AND DISCUSSION

In this paper we studied the phase transitions in the k -NN hard-core lattice-gas model on the triangular lattice. In this model, a particle excludes all the sites up to the k th next-nearest neighbors from being occupied by another particle. We obtained the phase diagram and quantified the critical behavior for $k \leq 7$ using the SCWL flat histogram algorithm, which incorporates rejection-free cluster moves to evolve the system.

We used the 1-NN model or the hard-hexagon model, for which an exact solution is known, to benchmark our simulations. For the 2-NN model, we obtained better estimates for the critical density. We showed that the 4-NN to 7-NN models undergo only a single first-order phase transition from a low-density disordered phase to a high-density sublattice-ordered phase. For each of these models, we obtained accurate estimates of the critical chemical potential, the densities of the disordered and sublattice phases in the coexistence regime, and the critical pressure. The quantitative results are summarized in Table III. The phase diagram in the μ - k plane and the ρ - k plane are shown in Fig. 20. Though μ_c on average increases with k [see Fig. 20(a)], we were unable to quantify the increase based only on results for $k \leq 7$. For the coexistence densities, with increasing k , we observed that ρ_s tends to 1 while ρ_f saturates around 0.8 [see Fig. 20(b)].

The results obtained in the paper allowed us to compare the efficacies of the TRG method and SCWL algorithm. The TRG method has been used to study the k -NN model on the triangular lattice [55]. The method yielded good results for $k = 1, 2, 3$. However, the results for 4-NN and 5-NN differed considerably from the results that we obtained using the SCWL algorithm. For the 4-NN model, the TRG method predicted a continuous transition. However, we showed clearly that the transition is first order. In addition, the extrapolated

TABLE III. Summary of the coexistence densities of the disordered phase ρ_f , the sublattice phase ρ_s , the critical chemical potential μ_c , and critical pressure P_c for different k . For $k = 1$, the results are exact [3,4]; the results for $k = 3$ are taken from Ref. [56].

k	ρ_f	ρ_s	μ_c	P_c
1		0.82917	2.4060	
2		0.7419(5)	1.7568(4)	
3	0.8482(1)	0.9839(2)	4.4641(3)	0.6397(1)
4	0.7404(2)	0.9067(2)	2.8696(2)	0.3262(2)
5	0.916(3)	0.988(3)	4.720(3)	0.3942(2)
6	0.7898(1)	0.9818(2)	4.2574(4)	0.3287(1)
7	0.7469(4)	0.9709(3)	3.9315(6)	0.2471(1)

critical chemical potential obtained in this paper does not lie in the range predicted by the TRG method for both $k = 4$ and $k = 5$. It would be of interest to see how the TRG method can be improved to be able to study a HCLG of particles with large excluded volume.

When k tends to infinity, the k -NN model resembles the hard-sphere model for which an intermediate hexatic phase separates a fluid and orientationally ordered high-density phase [75–80]. Thus, one would expect that signatures of these continuum phases are seen in the k -NN model for large enough k . The values of k for which the hexatic phase should be observable in the lattice model can be estimated as follows. In simulations of hard spheres in two dimensions, the hexatic phase is observed for packing fractions $\eta \in [0.716, 0.720]$ [78]. To observe the hexatic phase in a lattice model, the lattice spacing b should be such that it is able to resolve the mean void space between two spheres at the above range of packing fraction. The mean distance d between the centers of two spheres is $d \approx 2\sigma\sqrt{\eta_{\max}/\eta}$, where σ is the radius of the sphere and $\eta_{\max} = \pi\sqrt{3}/6$. Then the condition to observe the hexatic phase is

$$b \ll 2\sigma(\sqrt{\eta_{\max}/\eta} - 1) \approx 0.2477\sigma, \quad (21)$$

where we substituted $\eta = 0.718$, the mean packing fraction in the hexatic phase. For the k -NN model, the effective lattice

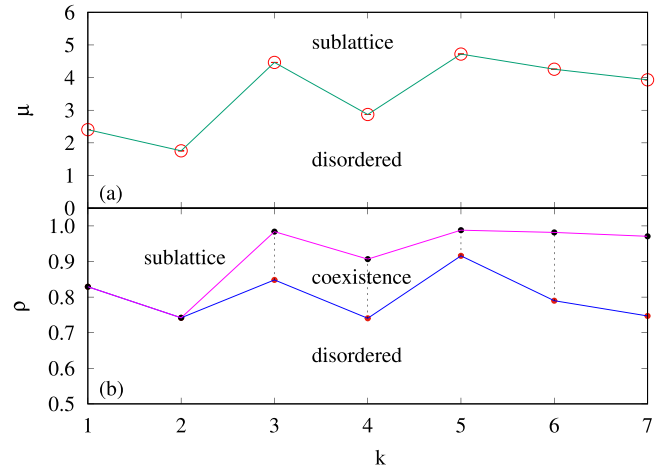


FIG. 20. Phase diagram of the k -NN model in the (a) μ - k plane and (b) ρ - k plane.

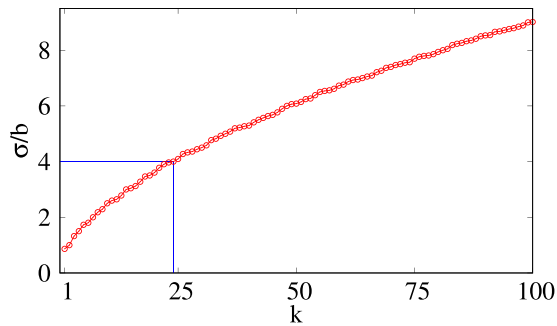


FIG. 21. Variation of σ/b , where σ is the radius of the sphere and b is the lattice spacing, with k for the k -NN model on the triangular lattice. The solid line, drawn based on Eq. (21), denotes the value of k beyond which a hexatic phase should be observable.

spacing for each k is easily computed and is shown in Fig. 21. Applying the condition in Eq. (21), we obtain that the hexatic phase should be observable in the lattice models for $k \gg 24$. This value of k is much larger than those that have been studied up to now and may possibly require more sophisticated algorithms to allow for equilibration. A similar analysis for the existence of a hexatic phase for the k -NN model on the square lattice gives $k \gg 28$.

The SCWL algorithm appears well suited to study phase transitions in HCLG models. The power of the flat histogram

method is amplified when applied to densities of states which depend on more than one variable. A viable example is the binary gas, the simplest of which is a mixture of 1-NN and 0-NN particles which shows a nontrivial phase diagram with a tricritical point [81–86]. Similarly, multidimensional densities of states appear in HCLG with additional attractive interactions [38,39,87–89]. In these models, it is possible to see a phase behavior similar to a Lennard-Jones fluid. However, the numerical studies suffer from both equilibration issues and the large parameter space to be explored. The basic idea of the SCWL flat histogram algorithm can be modified to analyze these models too. However, the determination of $C_0(n, \ell)$, the number of ways of placing n particles on a segment of length ℓ sites, is not as straightforward as was the case for the k -NN model. For binary or interacting gases, $C_0(n, \ell)$ will also depend on the configurations of neighboring rows and will have to be enumerated using transfer matrices, recursion relations, or similar techniques. These are promising areas for future study.

ACKNOWLEDGMENTS

The simulations were carried out on the high performance computing machine Nandadevi at The Institute of Mathematical Sciences Chennai, India and the computational facilities provided by the University of Warwick Scientific Computing Research Technology Platform.

- [1] L. K. Runnels, in *Phase Transitions and Critical Phenomena*, edited by C. Domb and M. S. Green (Academic Press, New York, 1972), Vol. 2, p. 305.
- [2] D. Frenkel, Entropy-driven phase transitions, *Physica A* **263**, 26 (1999).
- [3] R. J. Baxter, Hard hexagons: Exact solution, *J. Phys. A: Math. Gen.* **13**, L61 (1980).
- [4] R. J. Baxter, *Exactly Solved Models in Statistical Mechanics* (Academic Press, London, 1982).
- [5] A. Verberkmoes and B. Nienhuis, Triangular Trimers on the Triangular Lattice: An Exact Solution, *Phys. Rev. Lett.* **83**, 3986 (1999).
- [6] A. Bellemans and R. K. Nigam, Phase transitions in two-dimensional lattice gases of hard-square molecules, *J. Chem. Phys.* **46**, 2922 (1967).
- [7] K. Ramola and D. Dhar, High-activity perturbation expansion for the hard square lattice gas, *Phys. Rev. E* **86**, 031135 (2012).
- [8] T. Nath, D. Dhar, and R. Rajesh, Stability of columnar order in assemblies of hard rectangles or squares, *Europhys. Lett.* **114**, 10003 (2016).
- [9] J. Kundu and R. Rajesh, Phase transitions in a system of hard rectangles on the square lattice, *Phys. Rev. E* **89**, 052124 (2014).
- [10] J. Kundu and R. Rajesh, Phase transitions in systems of hard rectangles with non-integer aspect ratio, *Eur. Phys. J. B* **88**, 133 (2015).
- [11] B. C. Barnes, D. W. Siderius, and L. D. Gelb, Structure, thermodynamics, and solubility in tetromino fluids, *Langmuir* **25**, 6702 (2009).
- [12] A. Ghosh and D. Dhar, On the orientational ordering of long rods on a lattice, *Europhys. Lett.* **78**, 20003 (2007).
- [13] J. Kundu, R. Rajesh, D. Dhar, and J. F. Stilck, Nematic-disordered phase transition in systems of long rigid rods on two-dimensional lattices, *Phys. Rev. E* **87**, 032103 (2013).
- [14] N. Vigneshwar, D. Dhar, and R. Rajesh, Different phases of a system of hard rods on three dimensional cubic lattice, *J. Stat. Mech.* (2017) 113304.
- [15] D. Mandal, G. Rakala, K. Damle, D. Dhar, and R. Rajesh, Phases of the hard-plate lattice gas on a three-dimensional cubic lattice, *arXiv:2109.02611*.
- [16] G. Rakala, D. Mandal, S. Biswas, K. Damle, D. Dhar, and R. Rajesh, Spontaneous layering and power-law order in the three-dimensional fully-packed hard-plate lattice gas, *arXiv:2109.02619*.
- [17] J. Amar, K. Kaski, and J. D. Gunton, Square-lattice-gas model with repulsive nearest- and next-nearest-neighbor interactions, *Phys. Rev. B* **29**, 1462 (1984).
- [18] D. P. Landau and K. Binder, Phase diagrams and critical behavior of Ising square lattices with nearest-, next-nearest-, and third-nearest-neighbor couplings, *Phys. Rev. B* **31**, 5946 (1985).
- [19] K. Binder and D. P. Landau, Finite-size scaling at first-order phase transitions, *Phys. Rev. B* **30**, 1477 (1984).
- [20] P. A. Slotte, Phase diagram of the square-lattice Ising model with first- and second-neighbour interactions, *J. Phys. C* **16**, 2935 (1983).
- [21] C. Domb, Some theoretical aspects of melting, *Nuovo Cimento* **9**, 9 (1958).
- [22] D. M. Burley, A lattice model of a classical hard sphere gas, *Proc. Phys. Soc.* **75**, 262 (1960).
- [23] D. M. Burley, A lattice model of a classical hard sphere gas: II, *Proc. Phys. Soc.* **77**, 451 (1961).

- [24] A. Bellemans and R. K. Nigam, Phase Transitions in the Hard-Square Lattice Gas, *Phys. Rev. Lett.* **16**, 1038 (1966).
- [25] A. Bellemans and J. Orban, Phase Transition in a Lattice Gas with Extended Hard Core, *Phys. Rev. Lett.* **17**, 908 (1966).
- [26] J. Orban and A. Bellemans, Phase transitions in two-dimensional lattice gases of hard-core molecules. The triangular lattice, *J. Chem. Phys.* **49**, 363 (1968).
- [27] D. E. Taylor, E. D. Williams, R. L. Park, N. C. Bartelt, and T. L. Einstein, Two-dimensional ordering of chlorine on Ag(100), *Phys. Rev. B* **32**, 4653 (1985).
- [28] A. Patrykiewicz, S. Sokołowski, and K. Binder, Phase transitions in adsorbed layers formed on crystals of square and rectangular surface lattice, *Surf. Sci. Rep.* **37**, 207 (2000).
- [29] S. Mitchell, G. Brown, and P. Rikvold, Static and dynamic Monte Carlo simulations of Br electrodeposition on Ag(1 0 0), *Surf. Sci.* **471**, 125 (2001).
- [30] M. T. Koper, A lattice-gas model for halide adsorption on single-crystal electrodes, *J. Electroanal. Chem.* **450**, 189 (1998).
- [31] D.-J. Liu and J. W. Evans, Lattice-gas modeling of the formation and ordering of oxygen adlayers on Pd (1 0 0), *Surf. Sci.* **563**, 13 (2004).
- [32] Y. Zhang, V. Blum, and K. Reuter, Accuracy of first-principles lateral interactions: Oxygen at Pd(100), *Phys. Rev. B* **75**, 235406 (2007).
- [33] N. Bartelt, L. Roelofs, and T. Einstein, An unexpected low-coverage $c(2 \times 2)$ phase, *Surf. Sci. Lett.* **221**, L750 (1989).
- [34] E. Eisenberg and A. Baram, A first-order phase transition and a super-cooled fluid in a two-dimensional lattice gas model, *Europhys. Lett.* **71**, 900 (2005).
- [35] Z. Rotman and E. Eisenberg, Critical exponents from cluster coefficients, *Phys. Rev. E* **80**, 031126 (2009).
- [36] M. Weigt and A. K. Hartmann, Glassy behavior induced by geometrical frustration in a hard-core lattice-gas model, *Europhys. Lett.* **62**, 533 (2003).
- [37] M. Sellitto, First-order phase transition in a two dimensional BM_3 model, *J. Chem. Phys.* **156**, 124105 (2022).
- [38] J. Orban, J. Van Craen, and A. Bellemans, Lattice models of hard-core molecules with attractions: The phase diagram, *J. Chem. Phys.* **49**, 1778 (1968).
- [39] S. Prestipino and G. Costa, Condensation and crystal nucleation in a lattice gas with a realistic phase diagram, *Entropy* **24419** (2022).
- [40] R. J. Baxter, Planar lattice gases with nearest-neighbor exclusion, *Ann. Combin.* **3**, 191 (1999).
- [41] Y. Gurdal, J. Hutter, and M. Iannuzzi, Insight into (Co)pyrphyrin adsorption on Au(111): Effects of herringbone reconstruction and dynamics of metalation, *J. Phys. Chem. C* **121**, 11416 (2017).
- [42] T. Yokoyama, S. Yokoyama, T. Kamikado, and S. Mashiko, Nonplanar adsorption and orientational ordering of porphyrin molecules on Au(111), *J. Chem. Phys.* **115**, 3814 (2001).
- [43] T. Lelaidier, T. Leoni, A. Ranguis, A. D'aléo, F. Fages, and C. Becker, Adsorption and growth of bis-pyrene molecular layers on Au(111) studied by STM, *J. Phys. Chem. C* **121**, 7214 (2017).
- [44] P. Bak, P. Kleban, W. N. Unertl, J. Ochab, G. Akinci, N. C. Bartelt, and T. L. Einstein, Phase Diagram of Selenium Adsorbed on the Ni(100) Surface: A Physical Realization of the Ashkin-Teller Model, *Phys. Rev. Lett.* **54**, 1539 (1985).
- [45] H. C. M. Fernandes, J. J. Arenzon, and Y. Levin, Monte Carlo simulations of two-dimensional hard core lattice gases, *J. Chem. Phys.* **126**, 114508 (2007).
- [46] T. Nath and R. Rajesh, Multiple phase transitions in extended hard-core lattice gas models in two dimensions, *Phys. Rev. E* **90**, 012120 (2014).
- [47] N. T. Rodrigues and T. J. Oliveira, Husimi lattice solutions and the coherent-anomaly-method analysis for hard-square lattice gases, *Phys. Rev. E* **103**, 032153 (2021).
- [48] T. Nath and R. Rajesh, The high density phase of the k -NN hard core lattice gas model, *J. Stat. Mech.* (2016) 073203.
- [49] F. C. Thewes and H. C. M. Fernandes, Phase transitions in hard-core lattice gases on the honeycomb lattice, *Phys. Rev. E* **101**, 062138 (2020).
- [50] S. S. Akimenko, A. V. Myshlyavtsev, M. D. Myshlyavtseva, V. A. Gorbunov, S. O. Podgornyi, and O. S. Solovyeva, Triangles on a triangular lattice: Insights into self-assembly in two dimensions driven by shape complementarity, *Phys. Rev. E* **105**, 044104 (2022).
- [51] S. Darjani, J. Koplik, V. Pauchard, and S. Banerjee, Glassy dynamics and equilibrium state on the honeycomb lattice: Role of surface diffusion and desorption on surface crowding, *Phys. Rev. E* **103**, 022801 (2021).
- [52] G. S. Joyce, On the hard-hexagon model and the theory of modular functions, *Philos. Trans. R. Soc. A* **325**, 643 (1988).
- [53] N. C. Bartelt and T. L. Einstein, Triangular lattice gas with first- and second-neighbor exclusions: Continuous transition in the four-state Potts universality class, *Phys. Rev. B* **30**, 5339 (1984).
- [54] W. Zhang and Y. Deng, Monte Carlo study of the triangular lattice gas with first- and second-neighbor exclusions, *Phys. Rev. E* **78**, 031103 (2008).
- [55] S. S. Akimenko, V. A. Gorbunov, A. V. Myshlyavtsev, and P. V. Stishenko, Tensor renormalization group study of hard-disk models on a triangular lattice, *Phys. Rev. E* **100**, 022108 (2019).
- [56] A. A. A. Jaleel, D. Mandal, and R. Rajesh, Hard core lattice gas with third next-nearest neighbor exclusion on triangular lattice: One or two phase transitions?, *J. Chem. Phys.* **155**, 224101 (2021).
- [57] S. Darjani, J. Koplik, S. Banerjee, and V. Pauchard, Liquid-hexatic-solid phase transition of a hard-core lattice gas with third neighbor exclusion, *J. Chem. Phys.* **151**, 104702 (2019).
- [58] J. Kundu, R. Rajesh, D. Dhar, and J. F. Stilck, in *Solid State Physics: Proceedings of the 56th DAE Solid State Physics Symposium, Kattankulathur, 2011*, edited by R. Mittal, A. K. Chauhan, and R. Mukhopandhyay, AIP Conf. Proc. No. 1447 (AIP, Melville, 2012), p. 113.
- [59] K. Ramola, K. Damle, and D. Dhar, Columnar Order and Ashkin-Teller Criticality in Mixtures of Hard Squares and Dimers, *Phys. Rev. Lett.* **114**, 190601 (2015).
- [60] D. Mandal, T. Nath, and R. Rajesh, Phase transitions in a system of hard Y-shaped particles on the triangular lattice, *Phys. Rev. E* **97**, 032131 (2018).
- [61] N. Vigneshwar, D. Mandal, K. Damle, D. Dhar, and R. Rajesh, Phase diagram of a system of hard cubes on the cubic lattice, *Phys. Rev. E* **99**, 052129 (2019).
- [62] A. A. A. Jaleel, J. E. Thomas, D. Mandal, Sumedha, and R. Rajesh, Rejection-free cluster Wang-Landau algorithm for hard-core lattice gases, *Phys. Rev. E* **104**, 045310 (2021).

- [63] F. Wang and D. P. Landau, Efficient, Multiple-Range Random Walk Algorithm to Calculate the Density of States, *Phys. Rev. Lett.* **86**, 2050 (2001).
- [64] F. Wang and D. P. Landau, Determining the density of states for classical statistical models: A random walk algorithm to produce a flat histogram, *Phys. Rev. E* **64**, 056101 (2001).
- [65] R. Aveyard, R. Aveyard, and D. Haydon, *An Introduction to the Principles of Surface Chemistry* (Cambridge University Press, Cambridge, 1973).
- [66] S. Darjani, J. Koplik, and V. Pauchard, Extracting the equation of state of lattice gases from random sequential adsorption simulations by means of the Gibbs adsorption isotherm, *Phys. Rev. E* **96**, 052803 (2017).
- [67] M. E. Fisher, in *Critical Phenomena*, edited by F. J. W. Hahne, Lecture Notes in Physics (Springer, Berlin, 1983), Vol. 186, pp. 1–139.
- [68] H. E. Stanley, *Introduction to Phase Transitions and Critical Phenomena* (Oxford University Press, Oxford, 1971), Vol. 7.
- [69] N. Goldenfeld, *Lectures on Phase Transitions and the Renormalization Group* (CRC Press, Boca Raton, 2018).
- [70] F.-Y. Wu, The Potts model, *Rev. Mod. Phys.* **54**, 235 (1982).
- [71] J. Salas and A. D. Sokal, Logarithmic corrections and finite-size scaling in the two-dimensional 4-state Potts model, *J. Stat. Phys.* **88**, 567 (1997).
- [72] R. Blythe and M. Evans, The lee-yang theory of equilibrium and nonequilibrium phase transitions, *Braz. J. Phys.* **33**, 464 (2003).
- [73] I. Bena, M. Droz, and A. Lipowski, Statistical mechanics of equilibrium and nonequilibrium phase transitions: The Yang-Lee formalism, *Int. J. Mod. Phys. B* **19**, 4269 (2005).
- [74] See Supplemental Material at <http://link.aps.org/supplemental/10.1103/PhysRevE.106.044136> for further evidence of the first-order nature of the transition from the disordered phase to the sublattice ordered phase.
- [75] J. M. Kosterlitz and D. J. Thouless, Ordering, metastability and phase transitions in two-dimensional systems, *J. Phys. C* **6**, 1181 (1973).
- [76] A. P. Young, Melting and the vector Coulomb gas in two dimensions, *Phys. Rev. B* **19**, 1855 (1979).
- [77] D. R. Nelson and B. I. Halperin, Dislocation-mediated melting in two dimensions, *Phys. Rev. B* **19**, 2457 (1979).
- [78] E. P. Bernard and W. Krauth, Two-Step Melting in Two Dimensions: First-Order Liquid-Hexatic Transition, *Phys. Rev. Lett.* **107**, 155704 (2011).
- [79] M. Engel, J. A. Anderson, S. C. Glotzer, M. Isobe, E. P. Bernard, and W. Krauth, Hard-disk equation of state: First-order liquid-hexatic transition in two dimensions with three simulation methods, *Phys. Rev. E* **87**, 042134 (2013).
- [80] S. C. Kapfer and W. Krauth, Two-Dimensional Melting: From Liquid-Hexatic Coexistence to Continuous Transitions, *Phys. Rev. Lett.* **114**, 035702 (2015).
- [81] D. Poland, The coexistence curve for a mixture of hard-particle lattice gases, *J. Chem. Phys.* **80**, 2767 (1984).
- [82] T. J. Oliveira and J. F. Stilck, Transfer-matrix study of a hard-square lattice gas with two kinds of particles and density anomaly, *Phys. Rev. E* **92**, 032101 (2015).
- [83] D.-J. Liu and J. W. Evans, Phase transitions in mixed adsorbed layers: Effect of repulsion between “hard squares” and “point particles”, *J. Chem. Phys.* **114**, 10977 (2001).
- [84] N. T. Rodrigues and T. J. Oliveira, Three stable phases and thermodynamic anomaly in a binary mixture of hard particles, *J. Chem. Phys.* **151**, 024504 (2019).
- [85] N. T. Rodrigues and T. J. Oliveira, Thermodynamic behavior of binary mixtures of hard spheres: Semianalytical solutions on a Husimi lattice built with cubes, *Phys. Rev. E* **100**, 032112 (2019).
- [86] N. T. Rodrigues and T. J. Oliveira, Fluid-fluid demixing and density anomaly in a ternary mixture of hard spheres, *Phys. Rev. E* **101**, 062102 (2020).
- [87] W. Kinzel and M. Schick, Extent of exponent variation in a hard-square lattice gas with second-neighbor repulsion, *Phys. Rev. B* **24**, 324 (1981).
- [88] E. Aksenenko and Y. V. Shulepov, Multiphase behaviour of the plane quadratic lattice gas with nearest-neighbour exclusion and next-nearest-neighbour finite interaction, *J. Phys. A: Math. Theor.* **15**, 2515 (1982).
- [89] E. Aksenenko and Y. V. Shulepov, Extended cluster variation calculations for the plane quadratic lattice gas, *J. Phys. A: Math. Theor.* **17**, 2109 (1984).